Nonaxisymmetric Compressible Swirling Flow in Turbomachine Annuli

C. S. Tan* and E. M. Greitzer†
Massachusetts Institute of Technology, Cambridge, Massachusetts

The behavior of nonaxisymmetric disturbances in compressible swirling flows, typical of those found in turbomachine annuli, is examined using an analysis based on the Clebsch transformation of the equations of motion in reduced flow form. For the flows analyzed, the different types of disturbances (vorticity, entropy, and pressure) interact strongly in the presence of swirl. Numerical examples are presented to show that mean swirl level and mean Mach number can have a strong influence on the downstream evolution of the nonaxisymmetric disturbances. In particular, at high subsonic Mach number in regions of high swirl, nonaxisymmetric disturbances can show oscillations with decreasing amplitude as a function of downstream distance. A simple flow model is also used to examine the static pressure nonuniformities that can occur in one class of these nonaxisymmetric flows. The qualitative behavior described by this (much) simpler model is also deduced from the general analysis.

Nomenclature

c_p	= specific heat at constant pressure
$(\hat{e}_r,\hat{e}_\theta,\hat{e}_z)$	= unit vectors in r,θ,z coordinates
H	= enthalpy
$H(z)$	= unit Heaviside function
i	$=\sqrt{-1}$
M	= Mach number
P	= pressure
(r,θ,z)	= right-handed cylindrical coordinate system
S	= scalar used in velocity description
s	= entropy
T	= temperature
V	= absolute velocity vector
γ	= specific heat ratio
λ,Γ	= scalar used in velocity description
ρ	= density
τ	= drift function
τ_c	= stagnation temperature ratio across blade row
ϕ	= velocity potential
Ω	= vorticity

Subscripts

c	= convected quantity
n	= circumferential harmonic
p	= radial harmonic
R	= reduced flow
r,θ,z	= vector component in r,θ,z direction
t	= stagnation value
0	= simple radial equilibrium flow
$+\infty$	= far downstream station
$-\infty$	= far upstream station

Superscripts

d	= downstream
u	= upstream
$\tilde{(\ )}$	= periodic or circumferentially varying
$\bar{(\ )}$	= mean or axisymmetric

Received April 30, 1984; revision received March 1, 1985.
Copyright © American Institute of Aeronautics and Astronautics, Inc., 1985. All rights reserved.

*Research Associate, Department of Aeronautics and Astronautics.
†Professor, Director of Gas Turbine Laboratory, Department of Aeronautics and Astronautics. Associate Fellow AIAA.

I. Introduction

THE effect of inlet flow nonuniformities on the performance of turbomachines has been widely studied because of the detrimental effect on compressor stall margin and performance. In these studies, the distortions examined are often small enough so that a linearized treatment is possible. Linearized two-dimensional analyses of circumferentially distorted flow[1-3] yield these results: the vorticity disturbances associated with the flow nonuniformities are simply convected by the mean flow, and the static pressure field is thus potential. The vorticity and pressure disturbances are thus coupled only by boundary conditions and not through the structure of the flowfield.

If the inherently three-dimensional effects associated with a mean swirl are considered, however, the situation is quite different.[4-9] If there is a mean swirl (typical in turbomachine annuli once the flow has passed through one or more blade rows), the vorticity and the static pressure disturbances are *strongly coupled*. In such a situation, the three-dimensional disturbances may be classified into three types[6]: 1) exponentially decaying (irrotational), 2) purely convected (rotational), and 3) nonconvected (containing both rotational and irrotational parts). This implies that, as shown in Ref. 10, combined circumferential/radial distortion may not generally be able to be analyzed through the use of quasi-two-dimensional strip theory.

More recently, Goldstein[11,12] has presented analyses for the velocity field that results when small-amplitude vorticity and entropy disturbances are superposed on a steady, compressible potential flow. He has shown that, if the base flow is nonuniform, pressure disturbances will be created so that the pressure field cannot be decoupled from the vorticity and entropy fields.

In the present paper, the Clebsch description of the flow equations in reduced velocity form is used for analysis of steady, nonaxisymmetric disturbances due to stagnation pressure/temperature nonuniformity in a compressible, swirling flow environment. The reduced velocity approach is employed because it facilitates the direct application of the Clebsch formulation and solution procedure in a convenient form. In addition, the approach allows a useful interpretation of the flowfield in terms of a given solenoidal distribution of reduced vorticity, which can be directly determined in terms of the flow nonuniformities. Finally, results from a homentropic flow can be immediately adopted for the re-

duced flow obtained in a nonhomentropic flow. In the paper, calculations are also carried out to show the magnitudes of the effects to be expected in situations of practical interest.

II. Basic Aerothermodynamic Equations and Their Transformations

For the class of distortions under study, the upstream and downstream flow of the blade row can be taken as steady in the fixed coordinate system. It can be shown that, for a given steady flow of an ideal fluid in the absence of body forces, any other "reduced flow" determined by $V_R = V/\sqrt{F}$ and $\rho_R = F\rho$ will have the same streamlines if the scalar F is chosen so that it is conserved along streamlines, although it can vary from streamline to streamline.[9,13,14] For adiabatic inviscid flow, F can be taken to be a function of entropy or any of the stagnation properties of the fluid. The inertial forces, the pressure field, and the Mach numbers will also be the same in the two corresponding flows. Furthermore, the reduced and original flows satisfy the same kinematic boundary conditions at the boundaries.

For a perfect gas with constant specific heats, a useful choice of F is $F = e^{s/c_p}$ (Ref. 15). This transformation implies that there is a correspondence between a given nonhomentropic flow (V,ρ) and a homentropic reduced flow (V_R, ρ_R), and vice versa. The continuity and momentum equations in terms of the reduced flow quantities are

$$\nabla \cdot \rho_R V_R = 0 \tag{1}$$

$$V_R \times \Omega_R = \nabla \{H_t e^{-s/c_p}\} = \{c_p \nabla P_t^{(\gamma-1)/\gamma}\} \tag{2}$$

where the reduced vorticity Ω_R is defined by $\Omega_R = \nabla \times V_R$.

The reduced vorticity equation takes the form

$$V_R \cdot \nabla (\Omega_R/\rho_R) - (\Omega_R/\rho_R) \cdot \nabla V_R = 0 \tag{3}$$

The implication in the analogy between the equations for the reduced flow obtained from a nonhomentropic flow and a homentropic flow is that the analytical method used for homentropic flow is directly applicable to the reduced flow. Equation (3) implies that irrotationality of the reduced flow, once established, will persist. In contrast, the *nonhomentropic original flow*, even when starting uniformly from rest, *will not continue to be irrotational.* Equation (2) also implies that, as pointed out originally by Munk and Prim,[14] changes in the stagnation temperature distribution will not change the streamline pattern.

A general solution to Eq. (2) is given by

$$\Omega_R = \Omega_{\tau_R} + \Omega_{B_R} = \nabla \{c_p P_t^{(\gamma-1)/\gamma}\} \times \nabla \tau_R + \lambda_R V_R \tag{4}$$

where τ_R is the Darwin-Lighthill-Hawthorne drift function[17-19] satisfying

$$V_R \cdot \nabla \tau_R = 1 \tag{5}$$

in the *reduced flow*. Since $\Omega_{\tau_R} (= \nabla \{c_p P_t^{(\gamma-1)/\gamma}\} \times \nabla \tau_R)$, associated with the stagnation pressure variation, is divergence-free, the reduced Beltrami vorticity Ω_{B_R} satisfying the homogeneous equation $V_R \times \Omega_{B_R} = 0$ can be written as

$$\Omega_{B_R} = \nabla S_R \times \nabla \Gamma_R \tag{6}$$

If the stagnation pressure is constant, the reduced flow is either irrotational or a "reduced" Beltrami flow.[6] The variation of τ_R from streamline to streamline is directly connected with the development of streamwise reduced vorticity due to the stretching and tipping of the reduced vortex filaments associated with the stagnation pressure variation.

In the spirit of the Clebsch approach[16] to steady rotational flow, the reduced velocity vector V_R is decomposed into irrotational and rotational parts,

$$V_R = \nabla \phi_R + \{c_p P_t^{(\gamma-1)/\gamma}\} \nabla \tau_R + S_R \nabla \Gamma_R \tag{7}$$

where ϕ_R is the reduced velocity potential and $\{c_p P_t^{(\gamma-1)/\gamma}\} \nabla \tau_R$ and $S_R \nabla \Gamma_R$ are the parts of the reduced velocity vectors that account for the rotationality of the reduced flow.

The theoretical results are applied in the next section to analysis of the nonaxisymmetric disturbances caused by a steady pressure/temperature distortion. To the authors' knowledge, this is the first time an approach of this type has been applied to a nonaxisymmetric compressible flow in turbomachinery annulus.

III. Asymmetric Compressible Flow Through an Annular Blade Row

The asymmetric flow V under consideration (Fig. 1) is taken to be a small-amplitude distortion, $\tilde{v}$, superimposed upon a circumferentially averaged mean flow $\bar{V}$. This latter can be thought of as a sum of a simple radial equilibrium flow V_0 and an axisymmetric disturbance flow $\bar{v}$, associated with streamline curvature in the r-z plane.[21] Thus,

$$V = V_0 + (\bar{v}_r \hat{e}_r + \bar{v}_z \hat{e}_z) + \tilde{v} \tag{8}$$

where

$$V_0^{u,d} = \bar{V}_\theta \hat{e}_\theta H(z) + \bar{V}_{0_z}^{u,d} \hat{e}_z \tag{9}$$

The superscripts u and d denote the region upstream and downsteam of the annular blade row.

We take the variations in stagnation pressure or stagnation temperature (as well as the associated velocity $\tilde{v}$) to be small; i.e.,

$$\frac{|\tilde{v}|}{|V_0|}, \quad \frac{\delta P_t}{\frac{1}{2}\rho_0 V_0^2}, \quad \frac{c_p \delta T_t}{\frac{1}{2} V_0^2} = \mathcal{O}(\epsilon) \ll 1 \tag{10}$$

as well as $|\tilde{v}|/|V_0| \ll 1$. Thus, the stagnation quantities, the entropy, and (λ_R/ρ_0) remain constant on the streamlines of the simple radial equilibrium flow which, from the continuity condition, can be written as

$$\rho_0 V_0 = \nabla \alpha \times \nabla \psi \tag{11}$$

Without any loss of generality, we can choose $\alpha = \theta - f(r,z)$[5,6] so that ψ is the Stokes stream function for

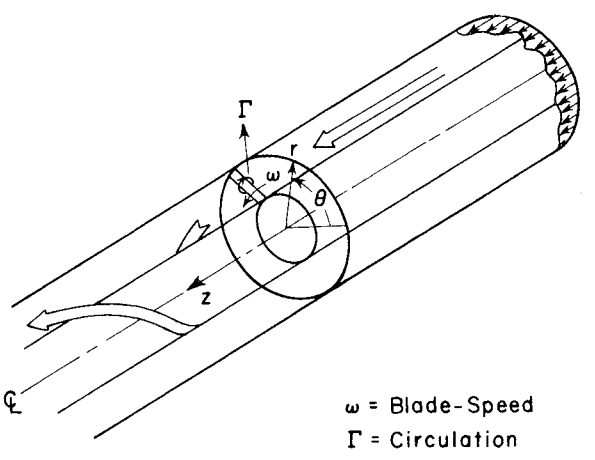

Fig. 1 Coordinate system for analysis of nonaxisymmetic flow through an isolated annular cascade.

V_0. For the present case, $f(r,z)$ is given by

$$f(r,z)=\int_0^z \frac{\bar{V}_\theta}{r\bar{V}_z}dz \simeq \left[\frac{\bar{V}_\theta}{V_{0z}}\frac{z}{r}\right]_{\text{along constant } \psi} \tag{12}$$

The solution and results presented here will be for the case of downstream free-vortex mean swirl; $\bar{V}_\theta = K_0/r$, where K_0 is a constant. For non-free-vortex swirl, a solution technique analogous to that in Ref. 6 can be employed.

From Eq. (7) it follows that, in the linearized approximation, the nonaxisymmetric disturbance flow can be described as follows:

$$\tilde{v}^u = (V_0^u/2)s^u + \nabla\phi_R^u + A_R^u \tag{13}$$

where

$$A_R^u = \left[1+\frac{\gamma-1}{2}\bar{M}_{z-\infty}^2\right]^{-[1/(\gamma-1)]}\tilde{P}_t^u\hat{e}_z \tag{14}$$

and

$$A_R^d = S_R(\alpha)\nabla\Gamma(\psi)+\frac{1}{\bar{V}_{z+\infty}}\left[1+\frac{\gamma-1}{2}\bar{M}_{z-\infty}^2\right]^{-[1/(\gamma-1)]} \times(\tau_c)^{-[1/(\gamma-1)]}\tilde{P}_t^d\hat{e}_z \tag{15}$$

All variables have been made dimensionless using $\rho_{-\infty}$, $V_{z-\infty}$, c_p, and r_t (tip radius). The rotationality in the upstream asymmetric flow is due to the imposed stagnation pressure variation; hence, Eq. (14). In the downstream region, the rotationality can be due to the presence of trailing vorticity from the blade row, the first term on the right-hand side of Eq. (15), as well as the stagnation pressure variation, in the first term on the right-hand side of Eq. (13) and the second term on the right-hand side of Eq. (15).

Equations for ϕ_R^u and ϕ_R^d can be derived from application of the continuity condition

$$L^u\phi_R^u = 0 \tag{16}$$

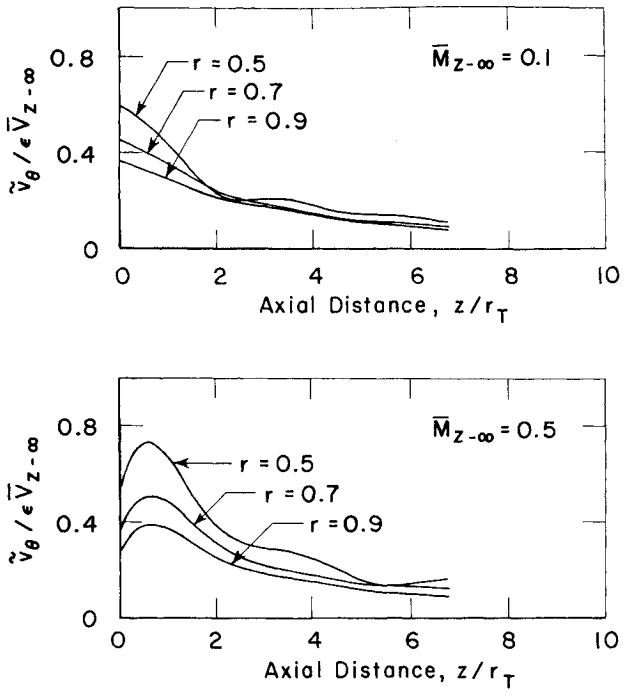

Fig. 2 Evolution of amplitude of tangential velocity perturbation downstream of stator for three radial locations.

$$L^d\phi_R^d = -\left\{\frac{1}{r}\frac{\partial}{\partial r}+\frac{\bar{M}_{\theta+\infty}^2}{r}\right\}\sum_{n=1}^{\infty}G_n(r)e^{in\alpha} + \frac{\{(1+(\gamma-1)/2\bar{M}_{z-\infty}^2)\tau_c\}^{-[1/(\gamma-1)]}}{r\bar{V}_{z+\infty}^2}\bar{V}_\theta\sum_{n=1}^{\infty}inP_n^d(r)e^{in\alpha} \tag{17}$$

In Eqs. (16) and (17) we have used the Fourier series representation

$$[\tilde{P}_t,\tilde{H}_t,\tilde{s},S_R(\alpha)\nabla\Gamma(\psi)] = \sum_{n=1}^{\infty}[P_n,H_n,s_n,G_n]e^{in\alpha} \tag{18}$$

The differential operators L^u and L^d are given by

$$L^u = \frac{\partial^2}{\partial r^2}+\frac{1}{r}\frac{\partial}{\partial r}+\frac{1}{r^2}\frac{\partial^2}{\partial\theta^2}+(1-\bar{M}_{z-\infty}^2)\frac{\partial^2}{\partial z^2} \tag{19}$$

$$L^d = \frac{\partial^2}{\partial r^2}+\frac{(1+\bar{M}_{\theta+\infty}^2)}{r}\frac{\partial}{\partial r}+\frac{(1-\bar{M}_{\theta+\infty}^2)}{r^2}\frac{\partial^2}{\partial\theta^2} -2\frac{\bar{M}_{z+\infty}\bar{M}_{\theta+\infty}}{r}\frac{\partial^2}{\partial\theta\partial z}+(1-\bar{M}_{z+\infty}^2)\frac{\partial^2}{\partial z^2} \tag{20}$$

Solutions to Eqs. (16) and (17) can be obtained in series of smooth eigenfunctions given by

$$\phi_R^u = \sum_{n=1}^{\infty}\sum_{p=1}^{\infty}A_{np}^u R_{np}^u(r)e^{in\theta}\begin{Bmatrix}e^{\lambda_{np}^u z}\\ e^{i\lambda_{np}^d z}\end{Bmatrix} + \sum_{n=1}^{\infty}\sum_{p=1}^{\infty}R_{np}^d(r)e^{in\theta}Z_{np}(z)H(z) \tag{21}$$

The eigenfunctions $R_{np}^{u,d}(r)$ are chosen to satisfy the boundary conditions at hub and tip of vanishing radial velocities. The solution procedure is sketched out in the Appendix and details can be found in Ref. 20.

Note that in the solution for ϕ_R from Eq. (17), $G_n(r)$, the contribution of the shed circulation to the downstream radial velocity, vanishes at hub and tip,[6,22] because the imposed upstream stagnation pressure distortion is taken to have vanishing radial derivative at the hub and tip.[10]

The first double sum in Eq. (21) is exponentially decaying but possibly oscillatory (complex λ_{np}). This is the potential type of disturbance that also exists in nonswirling flows. The second double sum is the nonconvected part of the disturbance, which changes as the fluid particle moves along the mean streamlines. A pressure field, and hence a coupling between pressure and entropy and/or vorticity disturbances, is associated with this type of disturbance. This behavior can be deduced from the functional form of $Z_{np}(z)$ given in the Appendix, which has, in the absence of swirl (to order ϵ) no contribution to the pressure field at all. Finally, the convected part of the disturbance flow, which has no associated pressure field, is given by $(V_0/2)s$ and A_R in Eq. (13).

The unknowns $\{A_{np}^u\}$, $\{G_n(r)\}$, $\{P_n^d(r)\}$, and $\{H_n^d(r)\}$ are determined through the application of matching conditions across the blade row, which we take to be an actuator disk. These are: 1) conservation of mass; 2) continuity of radial velocity; 3) constant leaving angle at the exit; 4) conservation of energy; 5) no loss across the blade row (i.e., isentropic flow).

Note that the linearized version of the velocity decomposition given in Sec. II is somewhat similar to that in Ref. 8. The decomposition used here, however, is in terms of the stagnation pressure and temperature, which are the quantities of interest in turbomachinery.

The above description of a three-dimensional disturbance field is rather general but is fairly complex. Thus, in the next section, we present a much simpler analysis which, although not as general, enables one to see the coupling of the pressure and vorticity/entropy disturbances explicitly.

IV. A Simple Theory for Static Pressure Nonuniformities in Compressible Swirling Flow

In this section, we develop a simple description of the three-dimensional swirling flow in an annular region in order to examine the static pressure nonuniformities that can occur. This description illustrates the coupling between pressure and entropy and/or vorticity perturbations, as well as the inherently three-dimensional secondary flow velocities driven by these pressure perturbations. Within the approximations made, it is shown that this quasi-three-dimensional description agrees with the more general approach.

For compressor response to steady inlet distortions, the nonuniformities associated with perturbations that have a wavelength equal to the circumference of the annulus are of most interest. The circumferential and axial length scale of such distortions in many situations is large compared to the annulus height. The flow at any circumferential position can thus be regarded as in *local* simple radial equilibrium, so that local radial pressure gradients are balanced by local centrifugal accelerations.[4] In addition, the mean flows considered are often not far from free vortex and the radial variation in entropy is not large. (The former restriction is actually not very severe, since the present type of analysis has been experimentally verified to give a very good description of a swirling flow with roughly constant values of $\bar{V}_\theta$, and $\bar{V}_z$, a situation quite different from a free vortex flow.)

With these approximations, the linearized equations of motion can be written as

$$-\frac{2\bar{V}_\theta \tilde{v}_\theta}{r} = -\frac{1}{\bar{\rho}}\frac{\partial \tilde{p}}{\partial r} + \frac{\tilde{\rho}}{\bar{\rho}}\left(\frac{1}{\bar{\rho}}\frac{\mathrm{d}\bar{p}}{\mathrm{d}r}\right) \tag{22}$$

$$\frac{\bar{V}_\theta}{r}\frac{\partial \tilde{v}_\theta}{\partial \theta} + \bar{V}_z\frac{\partial \tilde{v}_\theta}{\partial z} = -\frac{1}{\bar{\rho}r}\frac{\partial \tilde{p}}{\partial \theta} \tag{23}$$

$$\frac{\bar{V}_\theta}{r}\frac{\partial \tilde{v}_z}{\partial \theta} + \bar{V}_z\frac{\partial \tilde{v}_z}{\partial z} = -\frac{1}{\bar{\rho}}\frac{\partial \tilde{p}}{\partial z} \tag{24}$$

$$\frac{1}{\bar{\rho}r}\frac{\partial}{\partial r}(\rho r\tilde{v}_r) + \frac{1}{\rho}\frac{\bar{V}_\theta}{r}\frac{\partial \tilde{p}}{\partial \theta} + \frac{\bar{V}_z}{\rho}\frac{\partial \tilde{\rho}}{\partial z} + \left(\frac{1}{r}\frac{\partial \tilde{v}_\theta}{\partial r} + \frac{\partial \tilde{v}_z}{\partial z}\right) = 0 \tag{25}$$

$$\bar{V}_z\frac{\partial \tilde{s}}{\partial z} + \frac{\bar{V}_\theta}{r}\frac{\partial \tilde{s}}{\partial \theta} = 0 \tag{26}$$

In considering the effects due to a strongly swirling mean flow, it is useful to split the velocity field into three parts:[6]

1) The (circumferentially uniform) mean swirling flow.

2) That part of the velocity, density, etc., perturbations that can be taken to be convected along the mean streamlines. These would be the only perturbations that would occur if the mean flow were uniform.

3) "Secondary flow" perturbations arising from interactions between parts 1 and 2. These represent the fact that purely convected perturbations do not occur in this type of swirling flow.

Note that, in contrast to the analysis presented in Sec. III, neither the exponentially decaying potential flow disturbance nor the contribution from the trailing vorticity is included in this description. Hence, detailed matching at the blade row cannot be carried out, and we can only consider the downstream flowfield. However, the above decomposition of the velocity field is similar to that in Sec. III; the terms $(V_0/2)\tilde{s}^d$ and A_R in Eq. (13) correspond to that in part 2 above, while the second double sum in Eq. (21) corresponds to part 3 above.

The procedure followed is to expand the flow quantities in a Taylor series about conditions at the mean radius, $r=R$. This has been found to yield a quite useful description of the

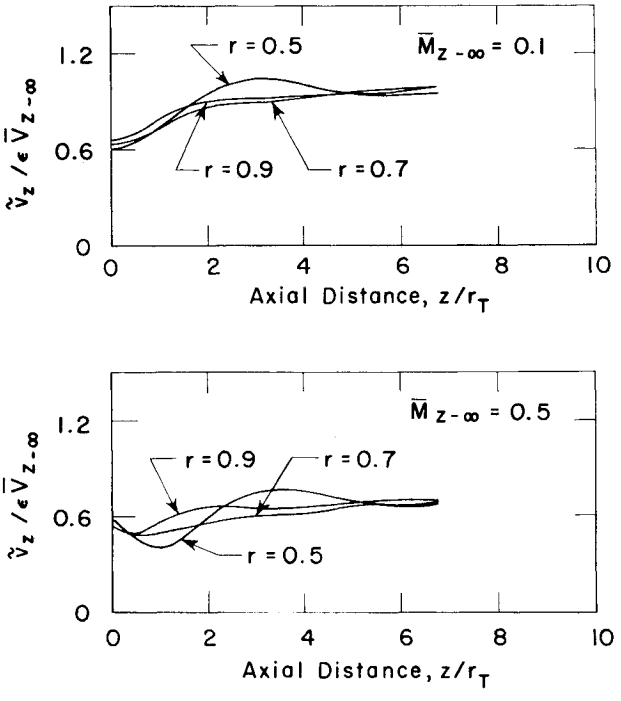

Fig. 3 Evolution of amplitude of axial velocity perturbation downstream of stator for three radial locations.

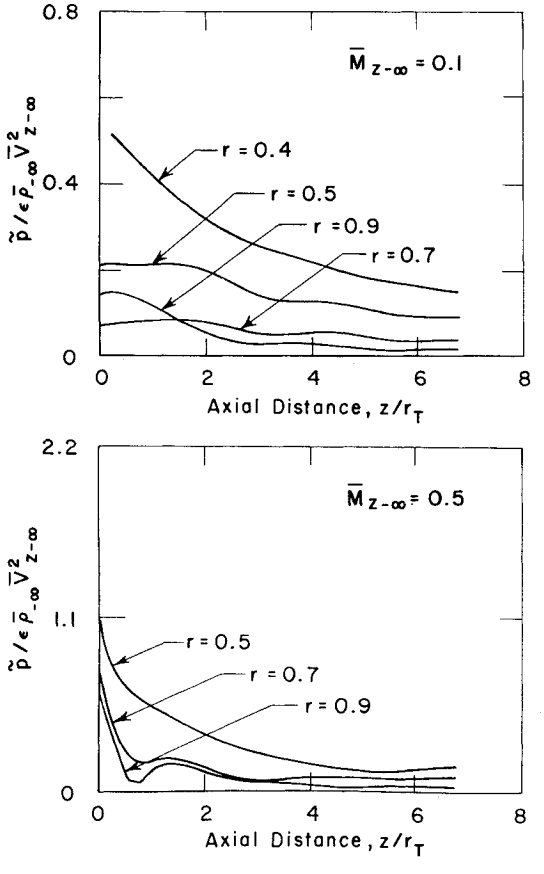

Fig. 4 Evolution of static pressure perturbation amplitude downstream of stator at various radii.

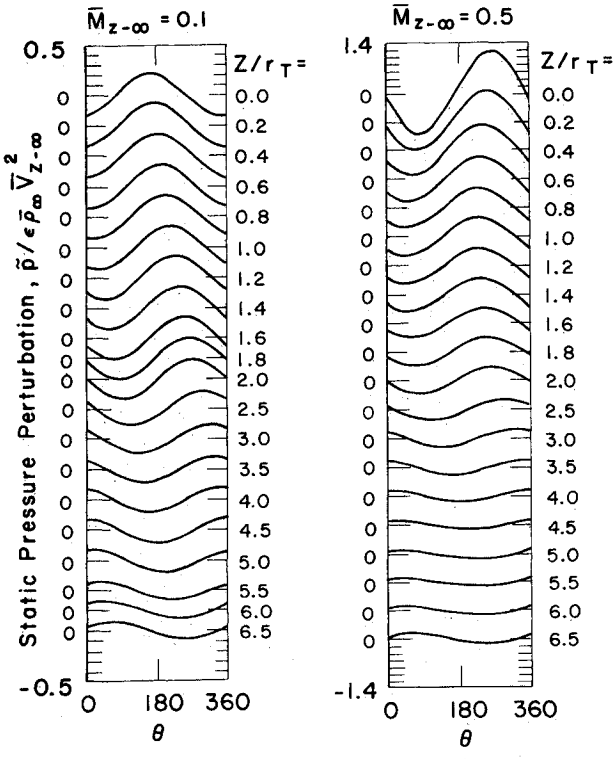

Fig. 5 Evolution of static pressure nonuniformity at $r=0.5$.

flow for the types of disturbances of interest. The leading term in this Taylor expansion is integrated using the assumption of local simple radial equilibrium to get an expression for the pressure,

$$\tilde{p}(r,z) = \rho\bar{V}_\theta^2 \frac{(r-R)}{R}\left(\frac{2\tilde{v}_{\theta_c}}{\bar{V}_\theta} - \frac{\tilde{s}_c}{c_p}\right)\Bigg|_{r=R} \tag{27}$$

where the quantities on the right-hand side are evaluated at the mean radius. The term $\tilde{v}_{\theta_c}$ is due to the vortical disturbance, whereas $\tilde{s}_c$ is associated with the entropy nonuniformity; both of these are convected with the mean flow. The presence of the entropy term actually reflects the effect of (convected) density perturbations since the entropy and density are related by

$$\tilde{s}_c/c_p = -\tilde{\rho}_c/\bar{\rho} \tag{28}$$

The pressure perturbations given in Eq. (27) are the driving terms for *secondary velocities* (denoted by subscript "1") $\tilde{v}_{\theta 1}$ and $\tilde{v}_{z1}$. These, in turn, can be found by integrating Eqs. (23) and (24) to give

$$\begin{Bmatrix} \tilde{v}_{\theta 1} \\ \tilde{v}_{z1} \end{Bmatrix} = -\frac{(r-R)}{R} z \frac{\bar{V}_\theta^2}{\bar{V}_z} \begin{Bmatrix} (1/R)(\partial/\partial\theta) \\ (\partial/\partial z) \end{Bmatrix} \left[\frac{2\tilde{v}_{\theta_c}}{\bar{V}_\theta} - \frac{\tilde{s}_c}{c_p}\right] \tag{29}$$

The derivatives of the quantity in square brackets are known since $\bar{V}_\theta$ and $\tilde{s}_c$ are specified at $z=0$ and are known functions of the variable $(\theta - z/R\tan\bar{\alpha})$. The convected part of the velocity perturbation terms ($\tilde{v}_{\theta c}$) correspond to vorticity disturbances and, *with a uniform base flow*, would thus represent a pure shear disturbance.

The pressure disturbances will have, within the context of the simple analysis, the same type of behavior as the vorticity and entropy disturbances in that they will also swirl around the annulus (at the mean flow angle) as one moves in the downstream direction. While the secondary flow velocities are predicted to increase linearly with downstream distance, their growth is in fact bounded since, at some downstream location, they will have grown large enough that the assumptions on which this simple analysis is based is no longer valid.[4]

It is of interest to examine how the simple model is related to the general results of the analysis in Sec. III. In Eq. (21), for $n=1$, small z and *small departure* from the mean radius R, the Taylor series of $Z_{1p}(z)$—hence $Z'_{1p}(z)$—about $z=0$ yields

$$\begin{Bmatrix} Z_{1p}(z) \\ Z'_{1p}(z) \end{Bmatrix} = \left(\frac{r-R}{R}\right)[\mu_p(R) + z\nu_p(R)] \tag{30}$$

where we have evaluated the value of the integrand at $r=R$ and replaced dr by $(r-R)/R$. It is these terms in the sum in Eq. (21) that represent the behavior of the nonconvected disturbances that are described by the simple model. In addition to the linear dependence on r about $r=R$, the nonconvected part of the velocity field has a linear dependence on z, the same as predicted by the simple model.

Finally, although we have expressed the static pressure perturbation and secondary flow velocities in terms of the vorticity and entropy distortions in Eq. (29), the former can also be expressed in terms of the nonuniformity in *stagnation pressure alone*[20] in accord with the general substitution principle of Munk and Prim.[14]

V. Numerical Examples

In this section, we present selected representative numerical results to show the effects of compressibility on the magnitude and downstream evolution of nonaxisymmetric disturbances in a swirling flow environment. In the first two examples, which are based on the general analysis, the distortion in stagnation pressure is specified at a station far upstream of a stator and a rotor, respectively. A third situation is then examined using the simple theory. For each example, only representative calculations are presented to illustrate the typical behavior; many other numerical results are given in Ref. 20.

In the calculations, only the Mach number in each example is varied, so that changes in disturbance behavior can be ascribed entirely to Mach number effects. The distortions to be considered are of the form

$$\tilde{p}_t = \epsilon\cos\theta \tag{31}$$

since it is the low-order disturbances that are most important in this problem. However, higher harmonics can also readily be examined within the framework of the present analysis.

The calculations are carried out for a free-vortex blade row representative of those in low hub-tip ratio turbomachines. The parameters used are

hub-to-tip ratio h = 0.4

$K_0/\bar{V}_{z+\infty}$ = 0.5 (corresponds to a swirl angle of about 35 deg at midradius)

stage loading Ψ (for rotor) = 0.6 [$\Psi = c_p\Delta T_t/(\text{rotor speed at mean radius})^2$]

ω (inverse of flow coefficient at blade tip) = $\begin{cases} 0 & \text{for stator} \\ 1.7 & \text{for rotor} \end{cases}$

In the calculations, the far upstream Mach number $M_{z-\infty}$ is varied so that the downstream Mach numbers vary from the incompressible regime to the high subsonic regime (i.e., ≥ 0.7).

In the following, velocity perturbations are nondimensionalized by $\epsilon V_{z-\infty}$, pressure perturbations by $\epsilon\rho_{-\infty}\bar{V}^2_{z-\infty}$, enthalpy perturbations by $\epsilon\bar{V}^2_{z-\infty}$, entropy by ϵc_p, and

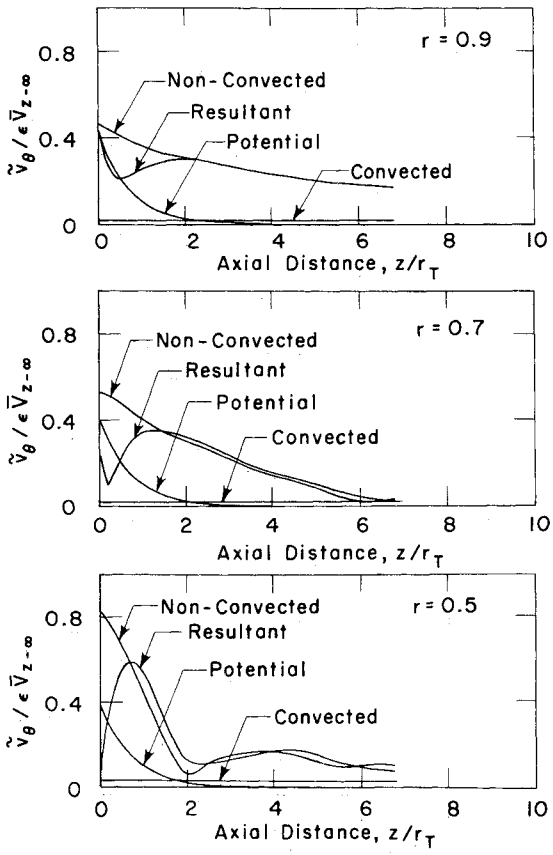

Fig. 6 Evolution of types of tangential velocity disturbance amplitude downstream of rotor at three radii; $\bar{M}_{z-\infty}=0.5$.

distance by tip radius r_T. The quantity r denotes the nondimensional radius, i.e., radius/r_T.

Stator (Inlet Guide Vane)

Figures 2 and 3 show the downstream evolution of the amplitude of the nonaxisymmetric velocity at different radii, for far upstream axial Mach numbers of 0.1 (essentially incompressible) and 0.5. The disturbance amplitude is plotted as a function of nondimensional downstream (axial) distance z ($z=0.0$ is the location of the blade row).

Figure 2 shows the amplitude of the *tangential velocity* perturbations. For $\bar{M}_{z-\infty}=0.1$, these decrease steadily with axial distance (Fig. 2a), but for $\bar{M}_{z-\infty}=0.5$, they increase to a maximum (at about $z=1$) before decreasing (Fig. 2b). In addition, the nondimensional amplitude is considerably larger at the higher Mach number.

The amplitude of the *axial velocity* perturbation is presented in Fig. 3. At $\bar{M}_{z-\infty}=0.1$ (Fig. 3a), the axial velocity amplitude in the outer part of the annulus increases until it reaches a steady value at $z\simeq 5.0$. This is due to the convected perturbations. For $r=0.5$ there is an increase, then a slight decrease, to this final value. For $\bar{M}_{z-\infty}=0.5$ (Fig. 3b), however, the amplitude decreases rather rapidly before following an oscillatory increase to the final value. The oscillations are strongest at $r=0.5$, where the swirl and Mach number are both high.

From the results in Figs. 2 and 3, it is noted that Mach number can have an influence on the downstream evolution of the amplitude of the velocity nonuniformities. In particular, the velocity tends to oscillate in the higher Mach number regime as well as in regions with larger swirl, i.e., the hub region. The explanation is that the different types of disturbance (potential, nonconvected, and convected) have different phases from one another in the θ-z plane at a particular radius [see Eq. (32)]. They thus combine to yield a resultant disturbance that has a different phase from that of each of the original component disturbances, and hence the amplitude varies with the downstream distance.

Figure 4 shows the behavior of the static pressure perturbation at $\bar{M}_{z-\infty}=0.1$ and 0.5. Although the compressibility does influence the behavior somewhat, the general trend is that oscillations in amplitude tend to decay strongly with downstream distance. This will be contrasted with the rotor behavior, which will be discussed below.

Figure 5 shows the downstream evolution of the static pressure perturbations at a given radius, i.e., static pressure vs circumferential position for different axial stations, at a constant radial location $r=0.5$. For low Mach number flow, the single-lobe asymmetric disturbance is seen to shift in the swirl direction. At $\bar{M}_{z-\infty}=0.5$, however, this shift (which can be characterized by the value of $d\theta/dz$ for the peak point of the perturbation) is much smaller for small downstream distances and, near the blade row, is actually opposite to the swirl direction. The reason is that

$$\frac{d\theta}{dz}=-\text{real part }(\lambda_{np}^{d})\text{for potential disturbances} \tag{32a}$$

$$\frac{d\theta}{dz}=\frac{K_0}{r^2\bar{V}_{z+\infty}}\text{for convected disturbances} \tag{32b}$$

$$\frac{d\theta}{dz}=\text{radial weighted average of }\frac{K_0}{r^2\bar{V}_{z+\infty}}$$
$$\text{for nonconvected disturbances} \tag{32c}$$

As $\bar{M}_{z-\infty}$ increases, the real part (λ_{np}) also increases, so that there is a stronger negative contribution to this shift from the potential disturbances. It is to be stressed that, although we have discussed the velocity and pressure distributions in terms of this shift, this is really an oversimplification, because the three types of disturbances have very different kinematic behavior.

Rotor

Before showing the numerical results for the rotor, some general discussion of the particular parametric studies that have been carried out is appropriate. The basic purpose of these studies was, as stated, to show the effect of compressibility on the behavior of nonaxisymmetric disturbances. To do this, the downstream Mach numbers should be in the high subsonic (say $M\geq 0.7$) regime. In an actual compressor this can occur when the upstream axial Mach number is relatively low because of the substantial contraction in annulus height that is generally present. The present analysis, however, treats only the case of constant annulus height. Hence, for a given upstream Mach number and stage loading, the downstream Mach numbers will be *substantially less* than those encountered in situations with annulus contraction. (This was not true for the vane row because of the velocity increase across the blade row.)

Thus, carrying out calculations at a value of $\bar{M}_{z-\infty}=0.5$, for example, is not sufficient to illustrate the significance of compressibility on the downstream flowfield. For this reason, we have done calculations using an upstream axial Mach number of $\bar{M}_{z-\infty}=0.9$, corresponding to a downstream resultant Mach number of about 0.75 at the hub and 0.45 at the tip. Although it is recognized that this is unrealistic from the points of view of 1) choking, and 2) nonisentropic behavior in a practical rotor, the *downstream flow evolution will still be correct* and the *downstream Mach numbers* will be more representative of those encountered in actual practice. The calculations will thus consist of cases with far upstream axial Mach numbers of 0.1 (essentially incompressible), 0.5, and 0.9.

The behavior of the velocity disturbance fields in the case of a rotor is qualitatively similar to that in a stator described

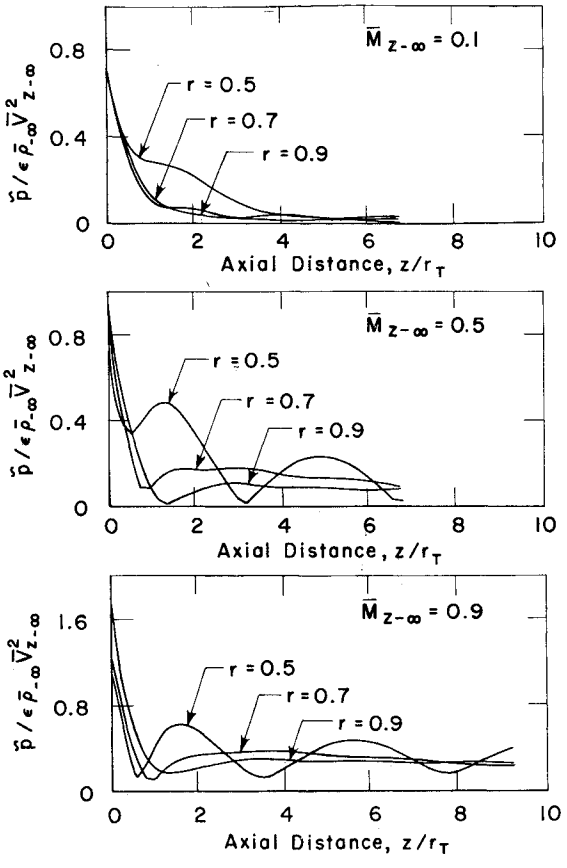

Fig. 7 Rotor: Evolution of static pressure perturbation amplitude downstream of rotor at three radii.

in the preceding sections on stators. However, to illustrate the difference in phase between potential, nonconvected, and convected parts of the disturbance, we present in Fig. 6 the downstream evolution of the amplitude of these different types of disturbances, as well as the resultant tangential velocity disturbance. (Other disturbance fields exhibit a similar behavior.) The graphs show this evolution at nondimensional radii of 0.9, 0.7, 0.5, respectively. The upstream Mach number is 0.5. At each radii, it is seen that the contribution from the convected part trends to be rather small while the potential part decays exponentially. At downstream distances greater than roughly one to two tip radii, the tangential velocity appears to be due mainly to the nonconvected disturbances. In the hub region, where larger swirl occurs, the amplitude of the nonconvected part and, hence, of the resultant tangential velocity perturbation tends to oscillate. The amplitude of the various disturbances do not add up to that of the resultant because of the difference in their phases.

Figure 7 shows the amplitude of the static pressure disturbance for different Mach numbers at $r=0.5$, 0.7, and 0.9. The static pressure nonuniformity decreases rapidly with z in the region very close to the blade row. The evolution at the higher Mach regime ($\bar{M}_{z-\infty}=0.5$, 0.9) is quite different (Figs. 7b and 7c). The amplitude of the static pressure disturbance increases markedly with the Mach number. In addition, near the hub, where the swirl is larger, the amplitude undergoes a decaying oscillation with downstream distance This is quite different from the behavior of the stator (Fig. 4), which has a far less oscillatory behavior. This can again be attributed to the difference in the phase of the tangential and axial velocity fields (between the stator and the rotor), which contributes to the resulting static pressure field. This phase difference is a consequence of the matching conditions across the rotor.

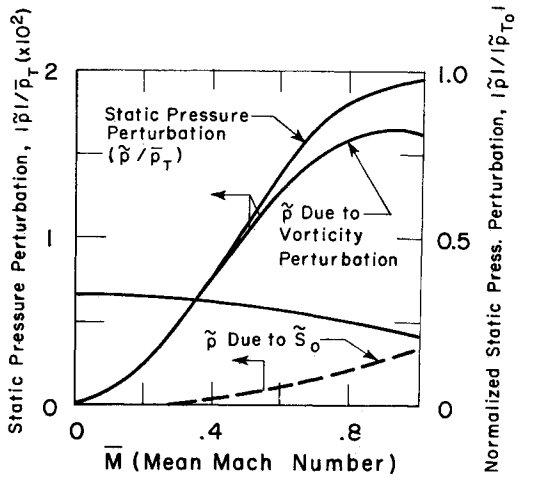

Fig. 8 Static pressure perturbations in an asymmetric compressible swirling flow computed from simple theory [$h=r_H/r_T=0.5$, $\bar{\alpha}=45$, $\bar{P}_{T_0}=0.25\ \gamma\bar{M}^2\bar{P}$].

The amplitude of the asymmetric disturbance thus tends to oscillate in regions of larger swirl and higher subsonic Mach number.

Numerical Example Using Simple Theory—Steady Circumferential Distortion

In this example, we take the mean swirl angle $\bar{\alpha}$ to be 45 deg, the hub/tip radius ratio of the annulus to be 0.5, and $|\tilde{p}_t|$ to be $\frac{1}{4}\rho\bar{V}_\infty^2$. The results are shown in Fig. 8 (note the difference in the nondimensionalizing scheme as compared to the previous example). The nondimensionalized static pressure nonuniformity $|\tilde{p}|/\bar{p}_t$ is plotted vs the mean Mach number $\bar{M}$. Also indicated on the figure are the respective contributions of the vorticity and entropy perturbations. On the right of the figure, the scale shows the static pressure normalized by the stagnation pressure nonuniformity $|\tilde{p}|/|\tilde{p}_t|$. The corresponding value from Ref. 6 (for incompressible flow) is given by the ordinate of this curve at $\bar{M}=0$. The variable plotted (i.e., $|\tilde{p}|/|\tilde{p}_t|$) has been chosen to illustrate directly the magnitudes of the effects.

There are several points to be made from the figure. First, and most obvious, the amplitude of the calculated static pressure nonuniformity increases strongly as $\bar{M}$ increases, simply because of the increase in the level of the dynamic pressure. Second, for many of the swirling flows that are of interest in turbomachines ($\bar{M}<1$), it is the vorticity disturbance that is most important, with the contribution of the entropy nonuniformity being relatively small.

It should be emphasized that this simple analysis does not include the exponentially decaying type of (potential) disturbance or the disturbances associated with the presence of the Beltrami vorticity. (Inclusion of these is the result of the matching conditions imposed at the disk.) Hence, the results obtained here cannot be compared directly with those obtained in Sec. III.

VI. Summary and Conclusions

The Clebsch approach to the aerothermodynamic equation of motion in a reduced flow has been applied to the study of the behavior of nonaxisymmetric disturbances in a compressible, strongly swirling flow environment, typical of those found in turbomachine annuli.

Entropy, vorticity, and pressure disturbances are strongly coupled in these swirling flows. Thus, in addition to convected and potential disturbances, nonconvected disturbances can also occur. These nonconvected disturbances are associated with a static pressure field that persists downstream with modulation in amplitude.

The numerical examples presented here show that compressibility can have a strong influence on the magnitude and downstream evolution of the nonaxisymmetric disturbance. In particular, at higher Mach number, the computed examples show that the amplitude of the disturbances in the hub region (where the swirl is the largest) tends to be larger. In this region the disturbance amplitude can also oscillate with decreasing modulation in the downstream direction.

At high Mach number, the potential disturbance can be dominant in the immediate neighborhood of the blade row. Thus there may be an initial rapid decay in disturbance magnitude followed by an increase, due to the presence of the nonconvected disturbances. At sufficiently high subsonic Mach numbers, the phase speed of the disturbance in θ-z space can be negative in the downstream region close to the blade row, becoming positive again further downstream.

Finally, it is noted that the differences between the results of the general analysis and the simple model can be attributed to the absence of the disturbances associated with the blade row matching conditions. It is, however, possible to extract from the more exact analysis the qualitative behavior of the nonconvected disturbance described by the simple model.

Appendix

The normalized eigenfunctions $R^u_{np}(r)$ are given by

$$R^u_{np}(r) = \left\{J_n(\chi_{np}r) - \frac{J'_n(\chi_{np})}{Y'_n(\chi_{np})} Y_n(\chi_{np}r)\right\} \div \left\{\int_h^1 r\left[J_n(\chi_{np}r) - \frac{J'_n(\chi_{np})}{Y'_n(\chi_{np})} Y_n(\chi_{np}r)\right]^2 dr\right\}^{1/2} \tag{A1}$$

J_n and Y_n are Bessel Functions of the first and second kind. The primes denote differentiation with respect to argument. The λ^u_{np} in Eq. (21) is given as

$$\lambda^u_{np} = \chi_{np}/\sqrt{1-\bar{M}^2_{z-\infty}} \tag{A2}$$

with χ_{np} determined from the transcendental equation

$$J'_n(\chi_{np})\,Y'_n(\chi_{np}h) - J'_n(\chi_{np}h)\,Y'_n(\chi_{np}) = 0 \tag{A3}$$

The radial eigenfunctions $\{R^d_{np}(r)\}$ of the downstream flowfield are chosen to satisfy

$$\frac{d^2R^d_{np}}{dr^2} + \frac{(1+\bar{M}^2_{\theta+\infty})}{r}\frac{dR^d_{np}}{dr} + \left\{2n\lambda^d_{np}A_{z\theta} - \lambda^{d2}_{np}B_{zz} - \frac{n^2}{r^2}(1-\bar{M}^2_{\theta+\infty})\right\}R^d_{np} = 0 \tag{A4}$$

and boundary conditions

$$\frac{dR^d_{np}}{dr} = 0 \quad \text{at } r = h,\ 1$$

$A_{z\theta}$ and $B_{z\theta}$ are approximated by

$$A_{z\theta} = \frac{m}{(1-h^m)}\int_h^1 r^{m-1}\left\{\frac{\bar{M}_{z+\infty}\bar{M}_{\theta+\infty}}{r}\right\}dr$$

$$B_{z\theta} = \frac{m}{(1-h^m)}\int_h^1 r^{m-1}(1-\bar{M}^2_{z+\infty})\,dr$$

instead of the original $\bar{M}_{z+\infty}\bar{M}_\theta/r$ and $(1-\bar{M}^2_{z+\infty})$. This approximation yields the relatively simple orthogonality condition

$$\int_h^1 \exp\left[\int \frac{1+\bar{M}^2_{\theta+\infty}}{r}dr\right]R^d_{np}(r)R^d_{nq}(r)\,dr = \begin{cases}\Lambda_{np} & \text{if } p=q\\ 0 & \text{otherwise}\end{cases} \tag{A5}$$

which allows $Z_{np}(z)$ in Eq. (21) to be obtained analytically as

$$Z_{np}(z) = -\frac{1}{B_{zz}\Lambda_{np}}\int_h^1 \left\{\left[r\frac{dF_{np}}{dr} - \bar{M}^2_{\theta+\infty}F_{np}\right]G_n(r) \times \exp\left[-in\frac{K_0}{\bar{V}_{z+\infty}}\frac{z}{r^2}\right]\right\} \div \left\{\left[\lambda^d_{np} - \frac{nK_0}{r^2\bar{V}_{z+\infty}}\right]\left[\lambda^{d*}_{np} - \frac{nK_0}{r^2\bar{V}_{z+\infty}}\right]\right\}dr - \frac{inK_0D_0}{\bar{V}_{z+\infty}B_{zz}\Lambda_{np}}\int_h^1 \left\{\frac{F_{np}P^d_n}{r}\exp\left[-in\frac{K_0}{\bar{V}_{z+\infty}}\frac{z}{r^2}\right]\right\} \div \left[\lambda^d_{np} - \frac{nK_0}{r^2\bar{V}_{z+\infty}}\right]\left[\lambda^{d*}_{np} - \frac{nK_0}{r^2\bar{V}_{z+\infty}}\right]dr \tag{A6}$$

where

$$F_{np}(r) = \exp\left[\int \frac{1+\bar{M}^2_{\theta+\infty}}{r}dr\right]\frac{R_{np}(r)}{r}$$

$$D_0 = \left\{\bar{V}_{z+\infty}\left[\left(1+\frac{\gamma-1}{2}\bar{M}^2_{z+\infty}\right)\tau_c\right]^{1/(\gamma-1)}\right\}^{-1}$$

and λ^{d*}_{np} is the complex conjugate of λ^d_{np}. The standard Galerkin's method is used for the determination of λ^d_{np} and $R^d_{np}(r)$ from Eq. (A4).

The value of m is chosen such that the λ^d_{np} from Eq. (A4) is the best approximation to the case when $A_{z\theta} = \bar{M}_{z+\infty}\bar{M}_\theta/r$ and $A_{zz} = (1-\bar{M}^2_{z+\infty})$. The governing equation for $Z_{np}(z)$ has been obtained by substitution of Eq. (21) into Eq. (17) and weighing the resulting equation with

$$\exp\left[\int \frac{1+\bar{M}^2_{\theta+\infty}}{r}dr\right]R^d_{np}(r)$$

Acknowledgments

This research, carried out in the Gas Turbine Laboratory, MIT, was supported by the Air Force Office of Scientific Research under Contract Number F49620-82-K-0002, Dr. J. D. Wilson, Program Manager. We thank Prof. E. E. Covert for his useful suggestions concerning the relation between the simple model and the general analysis. The helpful comments of Prof. F. E. Marble and Dr. N. A. Cumpsty are also appreciated.

References

[1] Ehrich, F., "Circumferential Inlet Distortion in Axial Flow Turbomachinery," *Journal of the Aeronautical Sciences*, Vol. 24, June 1957, pp. 413-17.

[2] Rannie, W. D. and Marble, F. E., "Unsteady Flows in Axial Turbomachines," ONERA, Comptes Rendus des Journées Internationales de Sciences Aéronautiques, Pt. 2, Paris, May 27-29, 1957, pp. 1-21.

[3] Plourde, G. A. and Stenning, A. H., "Attenuation of Circumferential Inlet Distortion in Multistage Axial Compressors," *Journal of Aircraft*, Vol. 5, March 1968, pp. 236-242.

[4] Greitzer, E. M. and Strand, T., "Asymmetric Swirling Flow in Turbomachine Annuli," *ASME Journal of Engineering for Power*, Vol. 100, Oct. 1978, pp. 618-629.

[5] Hawthorne, W. R., McCune, J. E., Mitchel, N. A., and Tan, C. S., "Non-Axisymmetric Flow Through an Annular Actuator Disc; Inlet Distortion Problem," *ASME Journal of Engineering for Power*, Vol. 100, 1978, p. 664.

[6] Tan, C. S., "Vorticity Modelling of Blade Wakes Behind Isolated Annular Blade-Rows: Induced Disturbances in Swirling Flows," *ASME Journal of Engineering for Power*, Vol. 103, No. 2, April 1981, pp. 279-287.

[7]Dunham, J., "Non-Axisymmetric Flows in Axial Compressors," *Mechanical Engineering Science*, Monograph No. 3, 1965.

[8]Kerrebrock, J. L., "Small Disturbances in Turbomachine Annuli with Swirl," *AIAA Journal*, Vol. 15, June 1977, pp. 794-803.

[9]Tan, C. S., "Three-Dimensional Vorticity-Induced Flow Effects in Highly Loaded Compressors," Ph.D. Thesis, Massachusetts Institute of Technology, Cambridge, June 1978.

[10]Lifshits, A., "Combined Radial Circumferential Inlet Distortion Through Highly-Loaded Annular Blade-Row," S.M. Thesis, Mechanical Engineering Dept., Massachusetts Institute of Technology, Cambridge, Sept. 1981.

[11]Goldstein, M. E., "Unsteady Vortical and Entropic Distortions of Potential Flows and Arbitrary Obstacles," *Journal of Fluid Mechanics*, Vol. 89, Pt. 3, 1978, pp. 433-468.

[12]Goldstein, M. E., "Turbulence Generated by the Interaction of Entropy Fluctuations with Non-Uniform Mean Flow," *Journal of Fluid Mechanics*, Vol. 93, Pt. 2, 1979, pp. 209-224.

[13]Hawthorne, W. R., "On the Theory of Shear Flow," MIT GTL Rept. No. 488, 1966.

[14]Munk, M. and Prim, R. C., "On the Multiplicity of Steady Gas Flows Having the Same Streamline Patterns," *Proceedings of the National Academy of Sciences*, Vol. 33, No. 55, 1947.

[15]Yih, C. S., *Dynamics of Non-Homogeneous Fluids*, MacMillan, New York, 1965.

[16]Lamb, H., *Hydrodynamics*, 6th ed., Cambridge University Press, London, 1932.

[17]Darwin, C., "Notes on Hydrodynamics," *Proceedings of the Cambridge Philosopical Society*, Vol. 49, pp. 342-354, 1953.

[18]Lighthill, M. J., "Drift," *Journal of Fluid Mechanics*, Vol. 1, Pt. 1, pp. 31-53, 1956; note also, "Corrigenda to Drift," *Journal of Fluid Mechanics*, Vol. 2, 1957, pp. 311-312.

[19]Hawthorne, W. R., "Engineering Aspects," Chap. 1, *Research Frontiers in Fluid Dynamics*, edited by R. T. Seeger and G. Temple, Interscience, New York, 1965.

[20]Tan, C. S. and Greitzer, E. M., "Non-Axisymmetric Compressible Flow Through Annular Actuator Disks," Masschusetts Institute of Technology, Cambridge, MA, MIT GTL Rept. 169, Dec. 1982.

[21]Hawthorne, W. R. and Ringrose, J., "Actuator Disk Theory of the Compressible Flow in Free Vortex Turbomachinery," *Proceedings of the Institute of Mechanical Engineers*, Vol. 178, Pt. 3I (ii), 1963-64, pp. 1-13.

[22]Smith, L. H., "Secondary Flow in Axial Flow Turbomachinery," *Transactions of the ASME*, Vol. 77, Oct. 1955, p. 1065.

From the AIAA Progress in Astronautics and Aeronautics Series...

LIQUID-METAL FLOWS AND MAGNETOHYDRODYNAMICS—v.84

Edited by H. Branover, Ben-Gurion University of the Negev
P.S. Lykoudis, Purdue University
A. Yakhot, Ben-Gurion University of the Negev

Liquid-metal flows influenced by external magnetic fields manifest some very unusual phenomena, highly interesting scientifically to those usually concerned with conventional fluid mechanics. As examples, such magnetohydrodynamic flows may exhibit M-shaped velocity profiles in uniform straight ducts, strongly anisotropic and almost two-dimensional turbulence, many-fold amplified or many-fold reduced wall friction, depending on the direction of the magnetic field, and unusual heat-transfer properties, among other peculiarities. These phenomena must be considered by the fluid mechanicist concerned with the application of liquid-metal flows in partical systems. Among such applications are the generation of electric power in MHD systems, the electromagnetic control of liquid-metal cooling systems, and the control of liquid metals during the production of the metal castings. The unfortunate dearth of textbook literature in this rapidly developing field of fluid dynamics and its applications makes this collection of original papers, drawn from a worldwide community of scientists and engineers, especially useful.

Published in 1983, 454 pp., 6×9, illus., $25.00 Mem., $55.00 List

TO ORDER WRITE: Publications Order Dept., AIAA, 1633 Broadway, New York, N.Y. 10019